

## Supporting information

### Versatile Polarization Generation with an Aluminum Plasmonic Metasurface

*Pin Chieh Wu,<sup>1,2</sup> Wei-Yi Tsai,<sup>2</sup> Wei Ting Chen,<sup>2</sup> Yao-Wei Huang,<sup>1</sup> Ting-Yu Chen,<sup>2</sup> Jia-Wern Chen,<sup>2</sup> Chun Yen Liao,<sup>2</sup> Cheng Hung Chu,<sup>1</sup> Greg Sun,<sup>3</sup> and Din Ping Tsai,<sup>1,2,4,\*</sup>*

<sup>1</sup> Research Center for Applied Sciences, Academia Sinica, Taipei 11529, Taiwan

<sup>2</sup> Department of Physics, National Taiwan University, Taipei 10617, Taiwan

<sup>3</sup> Department of Engineering, University of Massachusetts Boston, Boston, Massachusetts 02125, United States

<sup>4</sup> College of Engineering, Chang Gung University, Taoyuan 33302, Taiwan

\*[dptsai@phys.ntu.edu.tw](mailto:dptsai@phys.ntu.edu.tw)

#### 1. Optimization of SiO<sub>2</sub> layer thickness for the metasurface polarization generator

The dielectric spacer SiO<sub>2</sub> plays a key role in optimizing the polarization conversion. Its thickness separating the Al nanoantenna and underlying Al mirror affects their coupling strength which in turn determines the conversion efficiency, co-polarization reflectance, and absorption that are plotted in Fig. S1. It can be seen that when the SiO<sub>2</sub> thickness is around 50 nm, the Al-nanoantenna/SiO<sub>2</sub>/Al-mirror structure yields the highest polarization conversion efficiency over the visible range while suppressing co-polarization reflectance and absorption over the visible range (400-700 nm).

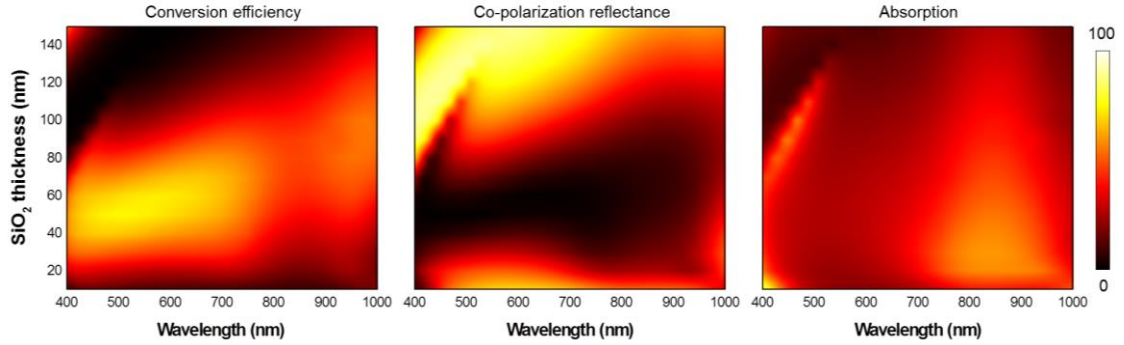


**Figure S1.** Simulated (Left) polarization conversion (cross-polarization) efficiency  $R_{\text{cross}}$  for circularly polarized light, (Middle) co-polarization reflectance  $R_{\text{co}}$  and (Right) absorption  $A = 1 - R_{\text{cross}} - R_{\text{co}}$  as a function of SiO<sub>2</sub> layer thickness and incident wavelength.

## 2. Fundamental resonances and half-wave plate behavior of Al nanoantenna

Here we illustrate in the top panel of Fig. S2(b) the fundamental resonances of Al nanoantenna in Fig. S2(a) under a normal illumination with linearly polarized light. For  $x$ -polarized light, a reflectance dip around 350 nm reveals its plasmon resonance along the short-axis of Al nanoantenna, while for  $y$ -polarized light, the first fundamental resonance along its long-axis appears around 850 nm. Between these resonances, an abrupt phase shift is induced as light scattering off from the metasurface consisting of Al nanoantennas. It can be seen from the bottom panel in Fig. S2(b) that the phase difference of  $180^\circ$  between the  $x$ - and  $y$ -polarized light spanning from around 400 to 770 nm is

obtained, indicating that the Al nanoantenna behaves as a half-wave plate over the visible range which is needed for the broadband circular polarization conversion.

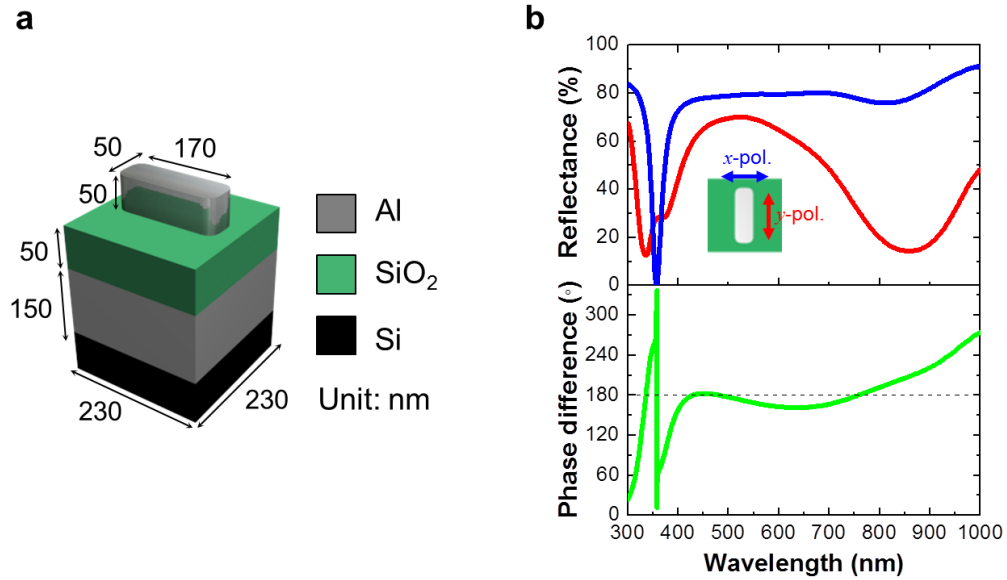


**Figure S2.** (a) Schematic for Al plasmonic nanoantenna. (b) Simulated (top) reflectance spectra for Al nanoantenna for  $x$ - and  $y$ -polarized normal illumination. Inset:  $x$ - and  $y$ -polarization relative to Al nanoantenna orientation. (Bottom) Phase difference for the  $x$ - and  $y$ -polarized scattered light.

### 3. sCOMS camera images

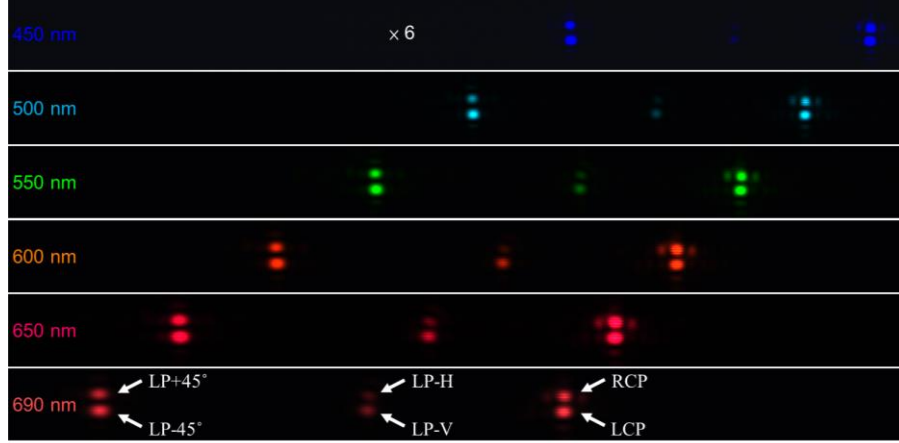


**Figure S3.** Camera images of six generated polarizing states. Generation of six polarizations from an incident LP-H wave at various incident wavelengths when the polarizer (P2) and quarter-wave plate are absent. These images are captured when six metasurface areas on a single chip are irradiated by a single incident beam.

### 4. Stokes parameters description via Mueller matrix

The Mueller matrix  $\mathbf{M}$ , which is a four-by-four matrix with real valued elements, can be used to describe the transformation of Stokes parameters of incident light into the scattered one when an incident light passes through a polarization altering component:

$$\mathbf{S}^s = \begin{bmatrix} S_0^s \\ S_1^s \\ S_2^s \\ S_3^s \end{bmatrix} = \mathbf{M}\mathbf{S}^i = \begin{bmatrix} m_{11} & m_{12} & m_{13} & m_{14} \\ m_{21} & m_{22} & m_{23} & m_{24} \\ m_{31} & m_{32} & m_{33} & m_{34} \\ m_{41} & m_{42} & m_{43} & m_{44} \end{bmatrix} \begin{bmatrix} S_0^i \\ S_1^i \\ S_2^i \\ S_3^i \end{bmatrix} \quad (\text{S1})$$

where  $\mathbf{S}^i$  and  $\mathbf{S}^s$  represent the Stokes vector of incident and scattered light, respectively. The Mueller matrix  $\mathbf{M}$  basically has different formalisms for different kinds of polarization altering components such as waveplate and polarizers etc. When a light beam passes through a sequence of polarization altering components, the resulting Mueller matrix  $\mathbf{M}$  can be directly obtained from the product of each individual matrix  $\mathbf{M}_i$

$$\mathbf{M} = \mathbf{M}_T \mathbf{M}_{T-1} \cdots \mathbf{M}_i \cdots \mathbf{M}_2 \mathbf{M}_1 \quad (\text{S2})$$

Based on the optical setup shown in Fig. 4c, the scattered light from MPG will pass through a quarter-wave plate then a linear polarizer. According to eq. S2, the final Stokes vector can be obtained by:

$$\frac{1}{2} \begin{bmatrix} 1 & 1 & 0 & 0 \\ 1 & 1 & 0 & 0 \\ 0 & 0 & 0 & 0 \\ 0 & 0 & 0 & 0 \end{bmatrix} \begin{bmatrix} 1 & 0 & 0 & 0 \\ 0 & \cos^2 2\varphi & \sin 2\varphi \cos 2\varphi & -\sin 2\varphi \\ 0 & \sin 2\varphi \cos 2\varphi & \sin^2 2\varphi & \cos 2\varphi \\ 0 & \sin 2\varphi & -\cos 2\varphi & 0 \end{bmatrix} \begin{bmatrix} S_0 \\ S_1 \\ S_2 \\ S_3 \end{bmatrix} \quad (\text{S3})$$

where  $\varphi$  is the angle of fast axis of quarter-wave plate. The intensity variation of scattered light from MPG can be subsequently obtained:

$$I(\varphi) = \frac{1}{2} S_0 + \frac{1}{4} S_1 - \frac{1}{2} S_3 \sin 2\varphi + \frac{1}{4} S_1 \cos 2\varphi + \frac{1}{4} S_2 \sin 2\varphi \quad (\text{S4})$$

Comprising eq. (S4) with eq. (4) in the main text, all Stokes parameters of scattered light from designed MPG can be subsequently obtained as  $S_0 = A - C$ ,  $S_1 = 2C$ ,  $S_2 = 2D$ ,  $S_3 = B$ .

## 5. Experimental verification of generated polarizing states cross the visible spectrum

range

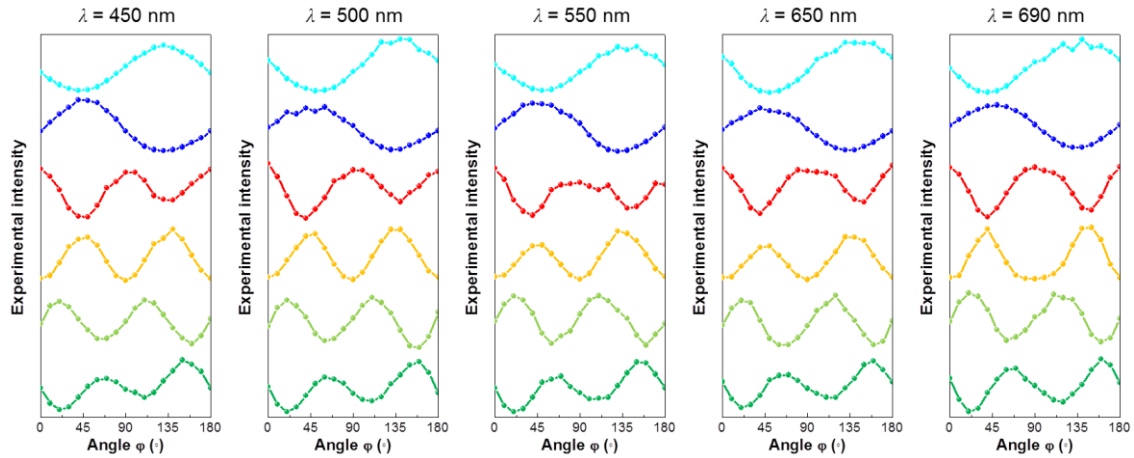


**Figure S4.** Experimental verification of generated polarizing states at different incident wavelengths. Experimental diagram of signal intensity as a function of rotating angle of the quarter-wave plate for different incident wavelengths.

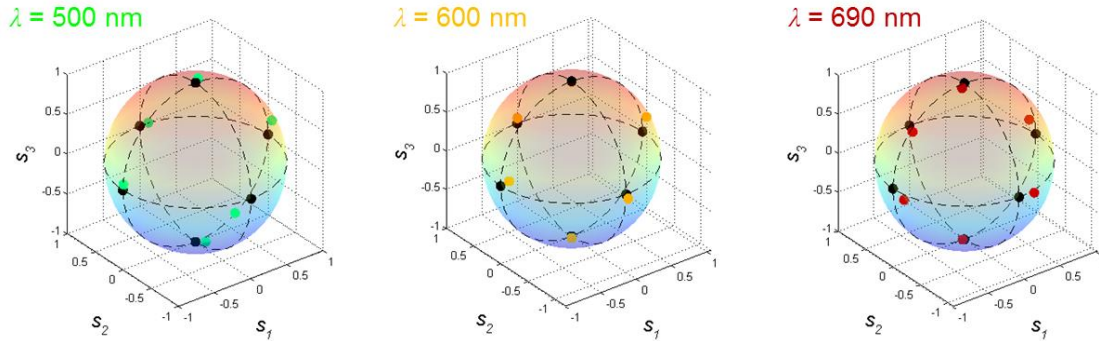


**Figure S5.** Poincaré sphere experimental results (color dots) compared with theoretical predictions (black dots) for incident wavelengths  $\lambda = 500, 600$  and  $690$  nm.